Ocean and Coastal Research

Case Report
Sousa, Carreira and Fonseca (Eds), Subsidies for ecosystem-based management in an offshore oil and gas exploration area, Santos Basin, Brazil
http://doi.org/10.1590/2675-2824071.2206icas

ISSN 2675-2824

Oceanographic conditions of the continental slope and deep waters in Santos Basin: the SANSED cruise (winter 2019)

Ilson C. A. da Silveira [1] *, Piero S. Bernardo [1], Cauê Z. Lazaneo [1], João P. M. Amorim [1], Milton Borges-Silva [1], Rafael C. Martins [1], Daniel M. C. Santos [1], Marcelo Dottori [1], Wellington C. Belo [2], Renato P. Martins [2], Luiz A. A. Guerra [2] and Daniel L. Moreira [2]

[1]Instituto Oceanográfico - Universidade de São Paulo, Praça Oceanográfico, 191 - Vila Universitaria, São Paulo - SP, 05508-120, [2]Centro de Pesquisas, Desenvolvimento e Inovação Leopoldo Américo Miguez de Mello - CENPES/PETROBRAS, Av. Horácio Macedo, 950 - Cidade Universitária da Universidade Federal do Rio de Janeiro, Rio de Janeiro - RJ, 21941-915
*Corresponding author: ilson.silveira@usp.br

Abstract

This work describes the circulation over the continental slope and the São Paulo Plateau in the Santos Basin during the SANSED winter 2019 survey. The cruise consisted of four legs in the period between June, 11 and August, 03 2019. The observed circulation is dominated by the Atlantic southwestern boundary current regime and remotely-generated anticyclones and cyclones. The former is composed by the Brazil Current, the Intermediate Western Boundary Current and their mesoscale meanders; the latter are 300km vortical rings with origin in the eastern side of the South Atlantic Basin. A Lagrangian scheme applied over satellite altimeter maps indicate that the origin of these rings is primarily the Cape Basin off South Africa. The interaction between the boundary currents, their cyclonic meanders, and the anticyclonic rings is complex, and varies widely. During the SANSED winter 2019 survey period, three anticyclones interacted with the Brazil Current, instabilizing it, forming dipoles with the current cyclonic meanders, leading to their downstream propagation. Ancienter cyclonic eddies within Santos Basin may interfere with the propagation of the large anticyclones further south. In addition, the continuous arrival of remotely-originated anticyclones, the larger portion over the São Paulo Plateau presented a tendency of counter-clockwise circulation during the whole cruise period.

Keywords: Brazil Current, Mesoscale eddies, Santos Basin dynamics

INTRODUCTION

The Santos Basin (SB) is limited in the north by the Cape Frio High (22°S) region, and in the south by the Cape of Santa Marta High (28.5°S). Geomorphologically, the deep water region is characterized by a gentle continental slope and the São Paulo Plateau (SPP). The latter feature replaces the continental rise within the SB (Zembruscki 1979). The SPP presents its broader width off the São Sebastião Island, and at the depth of approximately 2500 m (Evain et al. 2015). Hydrodynamically, the continental slope and deeper water circulation is complex and formed by both the western boundary current system and impinging mesoscale vortical features (Figure 1). These impinging eddies come mostly from the east, from the South Atlantic Basin interior.

Submitted: 31-May-2022
Approved: 21-Nov-2022
Associate Editor: Renato Carreira

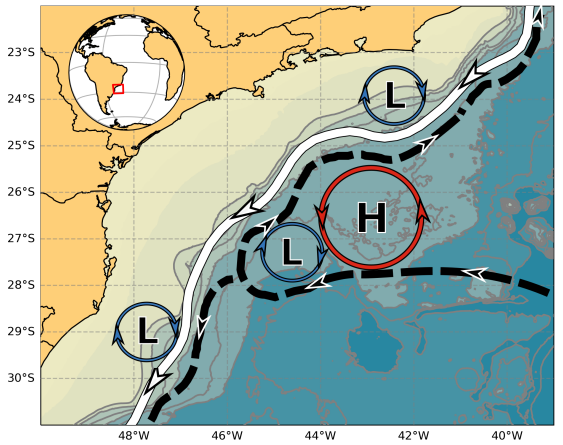

Figure 1. Schematic representation of the BC (white line) -IWBC (dashed black line) circulation system and the associated mesoscale activity (blue circles represent **L**ow-pressure center cyclones, and red are **H**igh-pressure center anticyclones) in Santos Basin. The eddies centered at 24°S and 29°S correspond to the Cape Frio Eddy and Cape Santa Marta Eddy, respectively. The vortical features over the SPP represent eddies coming from the eastern border of the South Atlantic.

The South Atlantic western boundary current within the SB is composed by the Brazil Current (BC), the Intermediate Western Boundary Current (IWBC), and their associated mesoscale activity. The BC is a surface-intensified current that extends down to 400-550 m transporting mainly Tropical Water (TW) and South Atlantic Central Water (SACW) poleward (Silveira et al. 2020). Its core, which can exceed 0.7 m s^{-1}, is on average found at the isobath of 1000 m (Silveira et al. 2008). The IWBC is an intermediate undercurrent which transports both Antarctic Intermediate Water (AAIW) and Upper Circumpolar Water (UCPW) equatorward. It occupies the 550-1300m depth portion typically. The IWBC core reaches 0.30 m s^{-1} at about 900 m, and coincides with the AAIW-related salinity minimum of the whole water column (Silveira et al. 2008). The IWBC formation occurs in the southern portion the SB through a bifurcation of the subpycnoclinic portion of the South Equatorial Current (SEC) – the Santos Bifurcation, as described by Böebel et al. (1999). These authors stated that the presence of the SPP imposes a cyclonic loop that starts the IWBC from the SEC northern branch. More recently, Luko et al. (2021) described that the SEC is formed by several separated bands and that the 30°S is the one that bifurcates, while the 26°S adds its transport integrally to the IWBC at intermediate levels. The AAIW-level at the SB southern portion is characterized by sluggish, intermittent flow (Müller et al. 1998) since it coincides with the Santos Bifurcation axis.

Both BC and IWBC transport about 4-6 Sv (1 Sv=10^6 m^3 s^{-1}), and set up a first-mode baroclinic jet, which can become unstable and develop eddies. Both Cape Frio and Cape Santa Marta ignite the meandering and cyclonic eddy formation from the BC-IWBC system. In particular, the so-called Cape Frio Eddy (CFE) is an unstable meander which grows quasi-stationarily just south of the Cape. The few observations of the CFE in the literature reveal that it extends from surface to the bottom over the slope, recirculating both the BC and IWBC cyclonically (Rocha et al. 2014). The formation of the CFE is far more recurrent than the Cape Santa Marta Eddy (CSME).

The remotely-originated component of the deep water circulation in the South Brazil Bight is formed by arriving anticyclones and cyclones. According to Laxenaire et al. (2018), the anticyclonic features have as primary source the Agulhas Current Retroflection, located off the southern tip of the African continent. Once shed, these eddies propagate westward and may face a series of topographic obstacles and nonlinear interactions. In other words, they are subject to processes of topographic blocking (sometimes only partially) and eddy-eddy interactions. The latter phenomena can yield eddy splitting and merging in their route toward the SB. Very few, such as the anticyclone history first described by Guerra et al. (2018), keep their integrity along its trajectory across the South Atlantic. Nevertheless, an abundant arrival of such features is observed throughout the year in the SB, and they actively interact with the BC-IWBC system and its meanders (subsequently formed rings) (Laxenaire et al. 2020).

This article aims to report the synoptic scenarios captured during the SANSED2019 deep-water (SANSED DW2019) survey, part of *Santos Project – The Santos Basin Regional Environmental Characterization* (PCR-BS) - coordinated by PETROBRAS.

This project has as its goal the oceanographic characterization of the SB environment. We will focus on the physical oceanographic conditions over the continental slope and deeper waters observed during the four legs of the SANSED DW2019 survey.

THE SANSED DW2019 CRUISE DATA SET

During the SANSED DW2019 campaign (Table 1), an oceanographic survey was conducted aboard the *R/V Ocean Stalwart* to characterize the hydrographic properties and the circulation of the SB (Figure 2).

Table 1. Names, dates, and number of stations of the surveys conducted at Santos Basin during the SANSED DW2019 campaign.

Name	Dates	Number of stations
Leg 1	June 11 - June 23	19
Leg 2	June 25 - July 07	13
Leg 3	July 11 - July 22	15
Leg 4	July 23 - August 03	14

Throughout the cruise, velocity was continually profiled with two Vessel-Mounted Acoustic Doppler Current Profilers (VM-ADCP, Teledyne RDI - 38 and 150 kHz) set to sample at 20 m and 9 m vertical bins, respectively. Data were processed using the Common Ocean Data Access System software (CODAS), following the guidelines of Firing (1995). Streamfunctions and non-divergent horizontal velocity fields were obtained from the VM-ADCP data following the method developed by Li et al. (2006).

Top-bottom CTD (Seabird) profiles were carried out on the continental slope of the SB and over the SPP, collecting conductivity, temperature and depth (pressure). CTD downcasts data were spike-removed, averaged into a 1 m bin, and smoothed using a 21-point Hanning filter. We used the Gibbs SeaWater (GSW) Oceanographic Toolbox of the Thermodynamic Equation of SeaWater TEOS-10 (McDougall & Barker 2011) to compute the recommended hydrological variables, which were conservative temperature, absolute salinity and neutral density.

Additionally, satellite observations were employed using the multisatellite altimetry Absolute

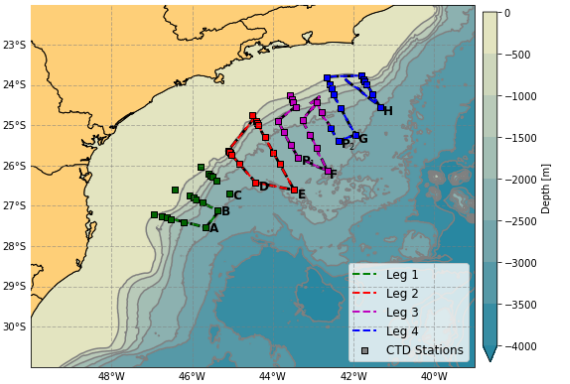

Figure 2. Map of the region surveyed by the SANSED DW2019 cruise legs. The colored lines represent the domain of observed velocities using VM-ADCP and the dots represent the CTD stations.

Dynamic Topography (ADT) Level 4 product and derived geostrophic currents and anomalies produced by the Seal Level Thematic Center (SL-TAC). This product spans from January 1993 to the present (near real time) and is distributed by Copernicus Marine Environment Monitoring Service (CMEMS, https://www.copernicus.eu/en). A general description of the product can be found on Pujol & Mertz (2019).

WATER MASS STRUCTURE

The region of the Brazil Current System, and consequently the SB, is composed by several water masses. For the study region, we focus on the portion of the first 3500 m of the water column. In this portion, we can find 6 water masses characteristics of the South Atlantic: TW, SACW, AAIW, UCPW, North Atlantic Deep Water (NADW) and Lower Circumpolar Water (LCPW) (Figure 3) (Silveira et al. 2000). Underneath these assemblages, there is the Antarctic Bottom Water (AABW) that extends to the bottom (Stramma & England 1999). Within the limits of Santos Sedimentary Basin, the sampling did not reach depths at which LCPW and AABW are found.

Water masses are formed in distinct regions and are characterized by typical temperature and salinity values, with a limit range at the interface between one type and another (Stramma & England 1999, Mémery et al. 2000, Silveira

et al. 2000). Therefore, in order to adopt a robust parameter that is unique for the analysis of water masses in the Santos Basin region, we used the neutral density surface analysis for the division of the regional water column (Jackett & McDougall 1997). This parameter takes hydrography and geographic position into account in the calculation. Thus, the isopycnal values representing the water mass interfaces are kept constant throughout all ocean basins. With the exception of the value referring to the TW-SACW interface, we followed the interfaces estimated by Valla et al. (2018) (Table 2).

According to Silveira et al. (2000), the TW has temperature greater than 20 °and salinity greater than 36 g kg^{-1}. Considering this temperature and salinity pair in the SB, the TW and SACW portions of the profiles related to the SANSED DW2019 cruise are better discriminated if considering the limit of 25.85 kg m^{-3}. When using the Valla et al. (2018) threshold (26.35 kg m^{-3}), some portions of the SACW were defined as TW, generating an erroneous interpretation of the data.

Also, due to the interaction of this layer with the atmosphere, this water is highly influenced by the fresh water and heat fluxes. Summarizing, the interval that defines this volume presents some variability, at least, a seasonal one. Therefore, the more specific the choice of this value, the more precise the division will be.

Table 2. Neutral density ranges of occurrence of South Atlantic water masses, according to Valla et al. (2018). The TW-SACW limit was revised for the present study.

Water Masses	Neutral Isopycnal range (kg m^{-3})
TW	< 25.85
SACW	25.85 - 27.10
AAIW	27.10 - 27.60
UCPW	27.60 - 27.90
NADW	27.90 - 28.10

Considering all the 67 profiles collected (6 of which were repeated stations) on the SANSED DW2019 cruise (Figure 2), we can observe the distribution of points between the density interval of the TW and NADW, considering the aforementioned water masses stacking sequence (Figure 3). From these profiles, we counted 80094 temperature and salinity measurements, of which 8.7% were classified as TW, 31.1% as SACW, 28.3% as AAIW, 22.5% as UCPW and 9.4% as NADW. More information about these water masses observed in the region can be found in the Table 3.

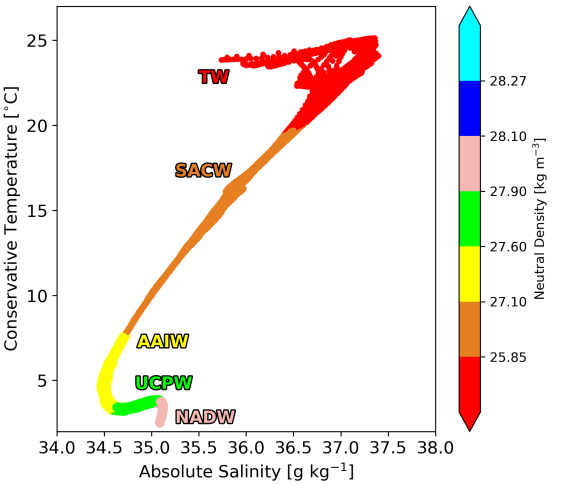

Figure 3. Temperature-Salinity Diagram for the observed CTD profiles during survey campaign. The color coding exhibits the portions of the diagram covered by each of the five water masses captured in SANSED DW2019:TW (red), SACW (orange), AAIW (yellow), UCPW (green), and NADW (carmine).

During the SANSED DW2019 survey, we observed three anticyclones interacting with the Brazil Current. With the general understanding of the average composition of the water masses observed in the SANSED DW2019 campaign, we will evaluate a case where the composition between the BC and of an anticyclonic vortical feature is comparable, in the same radial of the SB. In the Figure 4, the difference in the thermohaline composition of the BC and the anticyclone detected in leg 2 is evident (see the subpanel on Figure 4a), where the TW layer and the upper portion of the SACW (first 200 m) of the anticyclonic structure is warmer (+1.0 °C) and more saline (+0.2g kg^{-1}).

This difference is mainly due to the fact that the TW layer of the anticyclone profile is thicker (158 m) than that of the BC (109 m). If we compare with the values of the Table 3, we notice that this layer in the anticyclonic feature is larger than the average of

Table 3. Mean temperature ($\bar{T}$), mean salinity ($\bar{S}$), mean thickness ($\bar{H}$) and the mean depth of the top ($\bar{H}_{min}$) of each water masses (WM) for the Santos Basin.

WM	$\bar{T}$ (°C)	$\bar{S}$	$\bar{H}$ (m)	$\bar{H}_{min}$ (m)
TW	22.9±1.4	37.0±0.3	128.8±23.5	7.4 ±4.2
SACW	12.9±3.2	35.4±0.5	422.4±102.5	140.2 ±24.2
AAIW	4.8 ±1.2	34.6±0.1	459.2±177.2	620.3 ±47.2
UCPW	3.6 ±0.2	34.9±0.1	547.5±236.0	1192.9±38.0
NADW	3.4 ±0.3	35.1±0.0	308.2±240.1	1841.5±31.7

the region. The same occurs, respectively, for the SACW layer (450 m and 399 m), however, still close to the average values evaluated (Table 3). These curve misalignments may be an indication that the anticyclone is generated remotely.

The arrival of this anticyclone from the east (as it will be shown later in this work) brings a thicker TW layer and, consequently, more heat and salinity content than that observed in BC domain. Due to this thickening of the warmer and saline layers, the anomalies extend to the base of the AAIW layer (1190 m) of the anticyclone profile, with higher values, compared to the BC profile, of 1.0°C and 0.1 g kg^{-1} of salinity. Along with this difference, we can also observe a contrast in the homogeneity of these layers, by infering the density mean vertical gradient ($\frac{\partial \gamma}{\partial z}$) from the T-S diagram of Figure 4, the TW in the anticyclonic eddy profile (4.6×10^{-3} kg m^{-4}) is lower than that of BC (6.2×10^{-3} kg m^{-4}). i.e., the eddy, of origin external to the SB, is more mixed (or less stratified) than the BC. The difference extends to the SACW layers, but with a smaller discrepancy (3×10^{-4} kg m^{-4}), converging to a similar value (1.1×10^{-3} kg m^{-4}) in the AAIW layer.

EDDY ACTIVITY IN THE SANTOS BASIN

To describe the dynamic scenario of the mesoscale eddy-eddy and eddy-current interactions during the survey, we analyzed the data as follows: (i) compute horizontal distributions of near-surface streamfunction (ψ) derived from the VM-ADCP data; (ii) compare these maps with those of altimetry-derived Sea Surface Height (η) data set converted to streamfunction to enlarge the cruise area and better depict the features; and (iii) objectively interpolate the vertical structure of water column in terms of velocity.

We estimated the streamfunction through the non-divergent horizontal velocity field from the VM-ADCP using the Li et al. (2006) method. Geostrophic streamfunction from the altimeter dataset was obtained by simply removing the area mean value and converting it according to

$$\psi = -\frac{g}{f_0}\eta\,,$$

where f_0 is the Coriolis parameter evaluated at the SB central latitude of 26°S. In order to obtain vertical sections of neutral density and cross-transect velocities, we employed objective mapping with anisotropic Gaussian form following Silveira et al. (2004). We estimated from the sample correlation function the along-transect and vertical decorrelation lengths as being, on average, 33.41 km and 220.10 m respectively.

Since the basin presents high spatio-temporal variability due to the complex interactions between remote and locally-generated eddies, and meandering currents, we opt to analyze each leg separately (Figure 5).

Leg 1

Leg 1 was conducted in the southern SB centered in 27°S during June 11-23. This leg covered a small area in the south of the SB (Figure 5a). However, the horizontal surface circulation and the vertical section (Figures 5a, 5b and 5c) provided a glimpse of the presence of a mesoscale anticyclonic (hereafter AC1) feature attached to the BC flow. From the averaged streamfunction map derived from satellite data, we observe an overview of the circulation within the whole SB. In the north SB, we observed the meandering flow of the BC with the CFE on the cyclonic side of the jet and an anticyclonic eddy (hereafter AC2) over the SPP on the other side of the jet. The interaction between AC2, the CFE

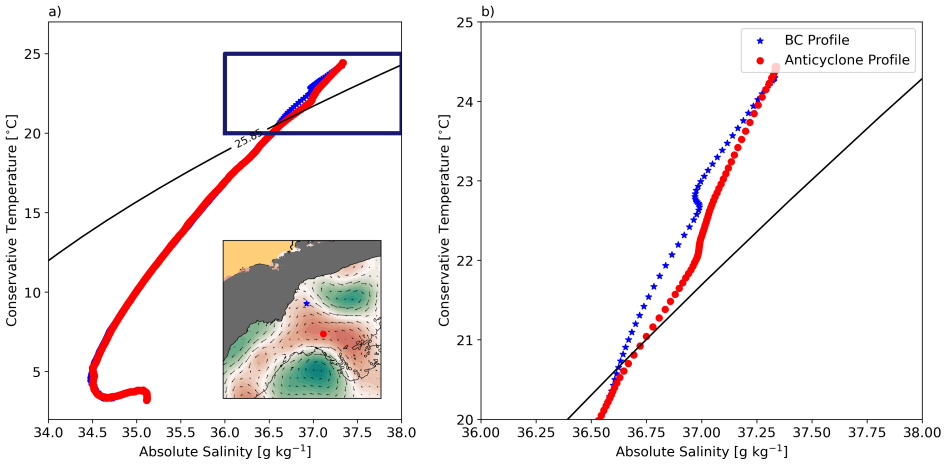

Figure 4. a) Comparison of the Temperature-Salinity profiles for the BC domain (blue) and an anticyclone (red); b) zoom in the TW domain (blue box on (a)), where the more important differences are noted. The 25.85 kg m^{-3} isopycnal marks the interface between TW and SACW. The map on (a) shows the location of the stations superimposed on the altimeter-derived geostrophic streamfunction.

and the cyclone (C1) of 100 km radius prevents the southwestern propagation of the AC2. To the west of this cyclonic feature, the AC1 is observed being pressed by the cyclone to the east and by the BC to the west. The elongated NE-SW orientated AC1 represents a merge of different anticyclonic eddies of probable remote origin. The shape of such elongated feature is driven by the northward propagation of the cyclonic eddy east of the elongated anticyclonic and the southward propagation of the CFE that follows the BC flow. Over this elongated anticyclonic signature we conducted the leg 1, which is depicted in Figure 5b. From the surface ADCP data we also sampled the AC1 signature confirming the presence of such feature from two independent data sources. Further, the vertical section in the northern edge of the leg 1 emphasizes the anticyclonic circulation and the presence of the AC1 attached to the BC flow (Figure 5c). The west lobe flow of the AC1 presents its core around 100 m above the continental shelf break, which matches the vertical level of the BC core towards the south. At this latitude, the BC is thicker than in the northern portion of the basin due to the southward branch of the Santos Bifurcation (Böebel et al. 1999, Luko et al. 2021), leading to a more barotropic vertical structure (Rocha et al. 2014).

Leg 2

Leg 2 occurred between June 26 and July 07 in the central part of the SB. At this portion of the basin we observed the westernmost branch of the CFE in the first 300 m of the water column (Figures 5d, 5e and 5f). Over the continental slope, there is the northward flow of the IWBC since the area comprised by this leg is in the north of the Santos Bifurcation (Böebel et al. 1999). The most prominent feature sampled in section E in leg 2 is the presence of the AC2 which has a sectional extension of approximately 200 km (Figure 5f). This feature occupies the entire water column sampled ($\sim$ 1250 m) confirming its relevant barotropicity. The estimated streamfunction from the VM-ADCP confirmed the presence of such anticyclone and the branch of CFE (Figures 5d and 5e). At this portion of the basin, we still observed the interaction of the BC with such eddies of both polarities concentrated over the SPP. In other words, the region presents a complex dynamics due to the influence of several geophysical processes, such as nonlinear eddy-eddy interactions.

Leg 3

Leg 3 was carried out between July 11 and 22, over a narrow region to the north of the sampled area in

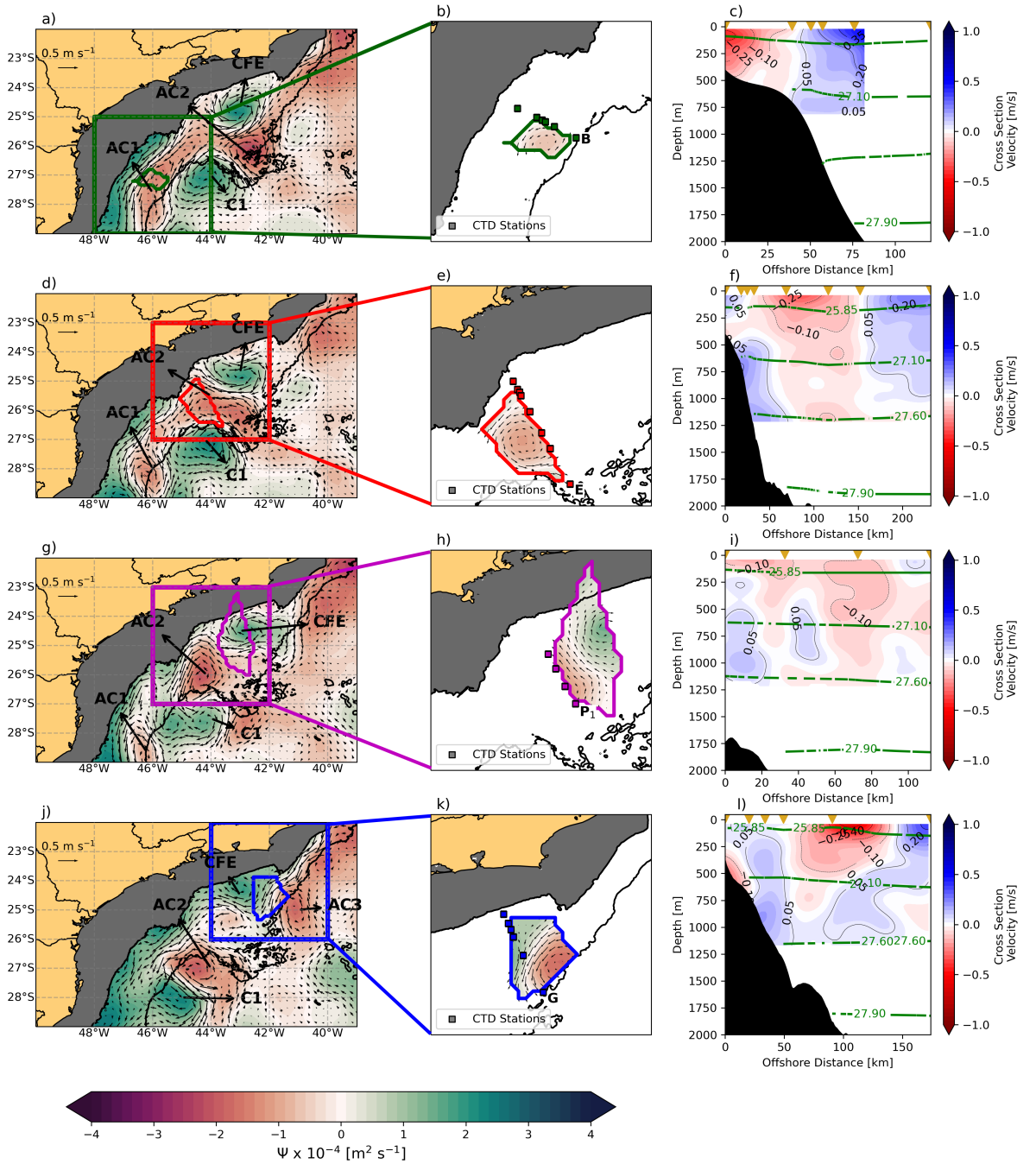

Figure 5. The circulation during the SANSED DW2019: Leg 1 (upper row), Leg 2 (second row), Leg 3 (third row), and Leg 4 (lower row). Left columns: altimeter-derived geostrophic streamfunction. Central columns: the near-surface *in-situ* streamfunction. Right columns: vertical sections of selected transects in each leg and isopycnals indicating the water masses interface following Valla et al. (2018). Gray shaded areas on the left and central columns indicate the isobaths of 150 and 2500 m.

leg 2 (Figures 5g, 5h and 5i). In this region, it was possible to observe a cyclonic lobe of the BC, which gives rise to the CFE and the northern lobe of the AC2 over the SPP (Figure 5g) described in the previous subsections. The most extended vertical section sampled in leg 3 (Figure 5i) highlights the complexity of the eddy-current interaction processes in the region. Since the sampled area represents a transitional region between two eddies of opposite polarities and the extension of the section is smaller than the radius of such eddies, it is expected to have the absence of an evident vertical structure pattern. However, the surface streamfunction indicates the dynamic influence of remotely-originated eddies on the BC system. During the period of leg 3, at least three mesoscale anticyclones and three mesoscale cyclones are present, distributed throughout the SB during the SANSED DW2019 survey (Figure 5g). The BC does not present a clear signature, since its flow has merged with AC2, centered at 25°S.

Leg 4

The last leg of the SANSED DW2019 cruise, over the continental slope and adjacent deep waters, took place between July 23 and August 3, south of Cape Frio (Figures 5j and 5k). From the non-divergent velocity field in the upper TW domain, we observed the presence of a mesoscale dipole limited at the center by the BC axis. On the cyclonic side of the BC, there is the CFE, formed by the BC meandering (Calado et al. 2006, Silveira et al. 2008) and on the anticyclonic side of the western boundary current, there is an anticyclonic eddy (AC3). Due to the presence of the dipole, the BC is locally intensified, followed by a downstream horizontal divergence. Such a configuration can lead to the energy conversion towards the inverse and the forward direction of the energy cascade.

To the south of the dipole region sampled in leg 4, it is still possible to observe the vortical features described in the previous legs. It means that in a short period of time ($\sim$ 2 months), an intense eddy activity was observed associated with the meandering BC and the anticyclonic eddies. The vertical structure of the opposite polarity eddies (Figure 5l) emphasizes the coupling of the vortical features, and the formation of the dipole. The result of such formation is the BC intensification and the deepening of the isopycnal in the eddy transition along the transect depicted in Figure 5l.

Origin of eddies off the Santos Basin

In the present subsection, we investigate if the anticyclonic eddies sampled in the SB during the SANSED DW2019 cruise possibly came from regions outside the domain region of the BC. That is, the anticyclonic vortical features are mainly westward propagating eddies that reach the SB and the Brazilian continental margin. In general, mesoscale isolated eddies tend to propagate westward, and the anticyclones specifically, have a longer lifetime, and consequently, they propagate over greater distances (Chelton et al. 2011).

In order to confirm that the anticyclonic eddies sampled in the SANSED DW2019 come from the Agulhas Retroflection, we performed Lagrangian experiments using the Ocean Parcels toolbox (Delandmeter & Sebille 2019) applied over daily sea surface height maps derived from multisatellite altimetry. The experiments consisted of releasing particles in the interior of the sampled eddies and advect them backward for a period longer than five years using geostrophic velocities anomalies from altimeters. Here we consider a period longer than five years as it represents a period longer than that documented by Guerra et al. (2018) for the crossing of an anticyclonic eddy through the South Atlantic Ocean basin. Considering that an anticyclonic eddy trajectory presents counter-clockwise loops in drifter trajectories (South Hemisphere) (Liu et al. 2015), we selected virtual particles that retained this pattern during the majority of the time. The results of the pathways indicate that the eddies' origin was indeed the Agulhas Current Region (Figure 6). It's important to note that during the trajectories, there are few moments in which the loop segments are lost. It is indicative of loss of coherence of the eddy structure, which may happen due to nonlinear interactions (splittings or mergings) (Wang et al. 2016). This procedure approaches the method applied by Laxenaire et al. (2018), which keeps tracking the eddies even after they undergo a nonlinear process like merging or split-ups. The limitation of the coverage period of the result pro-

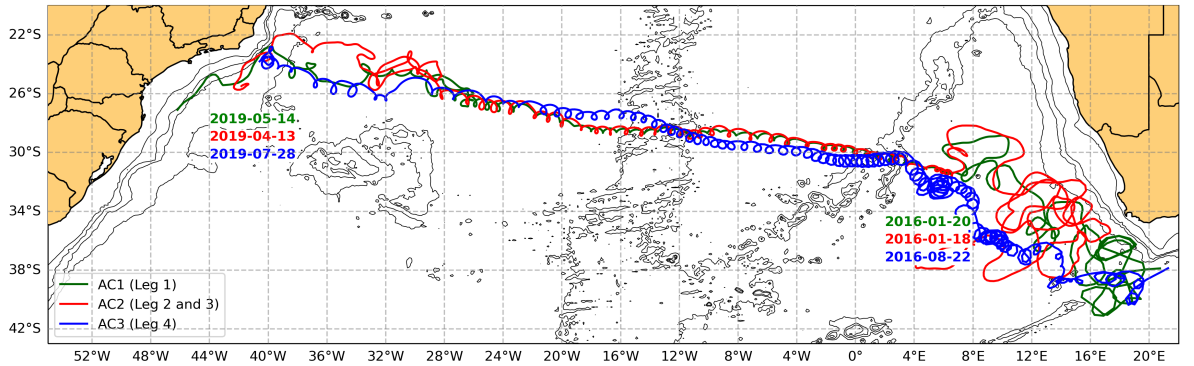

Figure 6. Trajectories of selected particles from Lagrangian experiments using geostrophic velocity anomalies from altimeter. The green trajectory represents the AC1 pathway, the red trajectory represents the AC2 pathway, and the blue trajectory represents the AC3 pathway. The dates represent the day that each particle crossed 4°E and 42°W respectively.

vided by the authors did not allow this data set to be used in the present work. However, as we observed the loss of loop segments along their pathways and observed a certain similarity of the structure of the water mass of the anticyclones with the local waters, we speculate that the eddies may have undergone nonlinear processes such as merging and split-ups.

Beyond these specific eddies, several others develop similar trajectories (Chelton et al. 2011, Laxenaire et al. 2018, Guerra et al. 2018, Nencioli et al. 2018). That is, they can be shed in the energetic retroflection region of the Agulhas Current and cross the Atlantic Ocean until collide with the BC on the extreme opposite side of the generation site.

SUMMARY AND FINAL REMARKS

In this study, we describe quasi-synoptic scenarios captured during the SANSED DW2019 cruise aiming to characterize the oceanographic conditions over the continental slope and adjacent deep waters of the SB. From a cruise divided into four stages during the austral winter of 2019, we observed an intense eddy activity in the SB. The eddy activity inherent to the BC has been widely reported in the literature. In particular, their generation north of the SB due to the presence of capes that changes the orientation of the continental margin (Calado et al. 2006, Silveira et al. 2008). Furthermore, it has been argued about the abundant arrival of remotely-originated eddies throughout the year in the SB, actively interacting with the BC-IWBC system and its meanders (Laxenaire et al. 2020). However, the effect of such interaction on the circulation of the SB is not well known.

Several mesoscale eddies of both polarities (anticyclonic and cyclonic) were captured in different regions of the SB but always associated with the BC poleward flow. Part of the observed eddies (mainly cyclonic eddies) is formed and pinched-off from the meandering BC. For example, the CFE is formed from an unstable BC meander, which grows primarily due to baroclinic instability (Silveira et al. 2008). The so-called quasi-stationarity of such an eddy seems to be broken by the arrival of the remotely-originated anticyclonic eddy. They eventually pair and initiate a dipole, a scenario that has been described by Guerra et al. (2018). The CFE may detach from the current further south, and both vortical features may keep propagating poleward. However, ancienter propagating eddies present in the central portion of the basin delay the propagation of newly shed eddies, especially when they pass through the SPP. Thus, a scenario of eddy-eddy interaction and eddy-current interaction formed by an array of eddies of both polarities interacting is configured.

The trajectories of such remotely-originated eddies observed in the SB during the survey confirmed that they were indeed pinched-off from the Cape Basin in the eastern South Atlantic Basin on the Agulhas Current domain. The geographical dis-

tance between these basins allows thermohaline differences in their contents, which is confirmed by Guerra et al. (2018) that claim that the eddies can cross the Atlantic Ocean without undergoing nonlinear processes and preserving their contents. On the other hand, nonlinear processes like splitting up and merging may occur with the eddies along their trajectories leading to a partial exchange of water mass content (Laxenaire et al. 2018, Nencioli et al. 2018).

In addition to the crossing of the sampled eddies, we speculated that the dynamics of the BC may be strongly affected by the input of the great mass, heat, and enstrophy carried by the anticyclonic eddies. However, a complete description and conclusion of the influence of these energetic eddies on the dynamics of the BC still need more detailed analysis. Our objective here was to present new *in situ* evidence of the dynamics of the BC in the SB domain are dominated by eddies during the winter of 2019. Here, the actors responsible for such complexity are due to the dynamics inherent to the meandering behavior of the BC itself, but mainly due to the connection with remotely-originated eddies.

ACKNOWLEDGMENTS

We thank CMEMS (http://www.marine.copernicus.eu) for the distribution of SSALTO/DUACS altimeter products. We thank Petróleo Brasileiro S.A. (PETROBRAS) for their permission to use and display the proprietary data from *Project Santos* for this paper. I.C.A.S., P.S.B. and C.Z.L. acknowledges support from CNPq (Project HIDROSAN I, 405593/2021-0) and FAPESP (Project HIDROSAN II, 2021/13124-6). We are indebted with Dr. Remi Laxenaire (University of La Réunion) for sending us the updated TOEddies results for 2010-2019, which were of great importance to carry out the interpretations presented in this article. We are also grateful to the two anonymous reviewers who helped to improve this manuscript quality.

REFERENCES

BÖEBEL, O., DAVIS, R. E., OLLITRAUT, M., PETERSON, R. G., RICHARD, P. L., SCHMID, C. & ZENK, W. 1999. The intermediate depth circulation of the Western South Atlantic, *Geophys. Res. Let.* **26**(21): 3329–3332.

CALADO, L., GANGOPADHYAY, A. & DA SILVEIRA, I. 2006. A parametric model for the Brazil Current meanders and eddies off southeastern Brazil, *Geophysical Research Letters* **33**(12).

CHELTON, D. B., SCHLAX, M. G. & SAMELSON, R. M. 2011. Global observations of nonlinear mesoscale eddies, *Progress in Oceanography* **91**(2): 167–216.

DELANDMETER, P. & SEBILLE, E. V. 2019. The Parcels v2. 0 Lagrangian framework: new field interpolation schemes, *Geoscientific Model Development* **12**(8): 3571–3584.

EVAIN, M., AFILHADO, A., RIGOTI, C., LOUREIRO, A., ALVES, D., KLINGELHOEFER, F., SCHNURLE, P., FELD, A., FUCK, R., SOARES, J. ET AL. 2015. Deep structure of the Santos Basin-São Paulo Plateau System, SE Brazil, *Journal of Geophysical Research: Solid Earth* **120**(8): 5401–5431.

FIRING, E. 1995. Processing ADCP data with the CODAS software system version 3.1, *Joint Institute for Marine and Atmospheric Research, University of Hawaii & National Oceanographic Data Center* .

GUERRA, L. A. A., PAIVA, A. M. & CHASSIGNET, E. P. 2018. On the translation of Agulhas rings to the western South Atlantic Ocean, *Deep Sea Research Part I: Oceanographic Research Papers* **139**: 104–113.

JACKETT, D. R. & MCDOUGALL, T. J. 1997. A neutral density variable for the world's oceans, *Journal of Physical Oceanography* **27**(2): 237–263.

LAXENAIRE, R., SPEICH, S., BLANKE, B., CHAIGNEAU, A., PEGLIASCO, C. & STEGNER, A. 2018. Anticyclonic eddies connecting the western boundaries of Indian and Atlantic Oceans, *Journal of Geophysical Research: Oceans* **123**(11): 7651–7677.

LAXENAIRE, R., SPEICH, S. & STEGNER, A. 2020. Agulhas Ring Heat Content and Transport in the South Atlantic Estimated by Combining Satellite Altimetry and Argo Profiling Floats Data, *Journal of Geophysical Research: Oceans* **125**(9): e2019JC015511.

LI, Z., CHAO, Y. & MCWILLIAMS, J. C. 2006. Computation of the streamfunction and velocity potential for limited and irregular domains, *Monthly weather review* **134**(11): 3384–3394.
URL: *https://doi.org/10.1175/MWR3249.1*

LIU, Z., DU, Y. & XU, K. 2015. An improved scheme of identifying loops using Lagrangian drifters, *2015 2nd IEEE International Conference on Spatial Data Mining and Geographical Knowledge Services (ICSDM)*, pp. 125–128.

LUKO, C., DA SILVEIRA, I., SIMOES-SOUSA, I., ARAUJO, J. & TANDON, A. 2021. Revisiting the Atlantic South Equatorial Current, *Journal of Geophysical Research: Oceans* **126**(7): e2021JC017387.

MCDOUGALL, T. J. & BARKER, P. M. 2011. Getting started with TEOS-10 and the Gibbs Seawater (GSW) oceanographic toolbox, *Scor/Iapso WG* **127**: 1–28.

MÉMERY, L., ARHAN, M., ÁLVAREZ-SALGADO, X. A., MESSIAS, M.-J., MERCIER, H., CASTRO, C. G. & RIOS, A. F. 2000. The water masses along the western boundary of the south and equatorial Atlantic, *Progress in Oceanography* **47**(1): 69–98.

MÜLLER, T. J., IKEDA, Y., ZANGENBERG, N. & NONATO, L. V. 1998. Direct measurements of western boundary currents off Brazil between 20°S and 28°S, *Journal of Geophysical Research: Oceans* **103**(C3): 5429–5437.

NENCIOLI, F., DALL'OLMO, G. & QUARTLY, G. D. 2018. Agulhas Ring Transport Efficiency From Combined Satellite Altimetry and Argo Profiles, *Journal of Geophysical Research: Oceans* **123**(8): 5874–5888.

PUJOL, M. & MERTZ, F. 2019. Product user manual for sea level SLA products, *Copernicus Marine Monitoring Service* .

ROCHA, C. B., SILVEIRA, I. C. A. D., CASTRO, B. M. & LIMA, J. A. M. 2014. Vertical structure, energetics, and dynamics of the Brazil Current System at 22°S–28°S, *Jounal Geophysical Research* **119**(1): 52–69.
URL: *http://dx.doi.org/10.1002/2013JC009143*

SILVEIRA, I. C. A. D., CALADO, L., CASTRO, B., CIRANO, M., LIMA, J. & MASCARENHAS, A. D. S. 2004. On the baroclinic structure of the Brazil Current–Intermediate Western Boundary Current system at 22°–23°S, *Geophysical Research Letters* **31**(14).

SILVEIRA, I. C. A. D., LIMA, J. A. M., SCHMIDT, A. C. K., CECCOPIERI, W., SARTORI, A., FRANSCISCO, C. P. F. & FONTES, R. F. C. 2008. Is the meander growth in the Brazil Current system off Southeast Brazil due to baroclinic instability?, *Dynamics of Atmospheres and Oceans* **45**(3): 187–207.

SILVEIRA, I. C. A. D., NAPOLITANO, D. C. & FARIAS, I. U. 2020. Water Masses and Oceanic Circulation of the Brazilian Continental Margin and Adjacent Abyssal Plain, *Brazilian Deep-Sea Biodiversity*, Springer, pp. 7–36.

SILVEIRA, I. C. A. D., SCHMIDT, A. C. K., CAMPOS, E. J. D., GODOI, S. S. & IKEDA, Y. 2000. A Corrente do Brasil ao largo da costa leste brasileira, *Revista Brasileira de Oceanografia* **48**(2): 171–183. In Portuguese.

STRAMMA, L. & ENGLAND, M. 1999. On the water masses and mean circulation of the South Atlantic Ocean, *Journal of Geophysical Research: Oceans* **104**(C9): 20863–20883.

VALLA, D., PIOLA, A. R., MEINEN, C. S. & CAMPOS, E. 2018. Strong mixing and recirculation in the northwestern Argentine Basin, *Journal of Geophysical Research: Oceans* **123**(7): 4624–4648.

WANG, Y., BERON-VERA, F. J. & OLASCOAGA, M. J. 2016. The life cycle of a coherent Lagrangian Agulhas ring, *Journal of Geophysical Research: Oceans* **121**(6): 3944–3954.

ZEMBRUSCKI, S. 1979. Geomorfologia da margem continental sul brasileira e das bacias oceânicas adjacentes, *PROJETO REMAC*, PETROBRAS. CENPES. DINTEP (Série REMAC no. 7), Rio de Janeiro, pp. 129–177.